University of Bristol - Explore Bristol Research
General rights
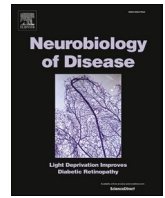
Deficient thyroid hormone transport to the brain leads to impairments in axonal caliber and oligodendroglial development

Víctor Valcárcel-Hernández [a], Daniela López-Espíndola [a,b], Marina Guillén-Yunta [a], Ángel García-Aldea [a], Inés López de Toledo Soler [a], Soledad Bárez-López [a,c,*], Ana Guadaño-Ferraz [a,**]

[a] *Department of Endocrine and Nervous System Pathophysiology, Instituto de Investigaciones Biomédicas Alberto Sols, Consejo Superior de Investigaciones Científicas (CSIC)-Universidad Autónoma de Madrid (UAM), Arturo Duperier 4, 28029 Madrid, Spain*
[b] *Escuela de Tecnología Médica and Centro de Investigaciones Biomédicas (CIB), Universidad de Valparaíso, Angamos 655, Reñaca, Viña del Mar, Chile*
[c] *Translational Health Sciences, Bristol Medical School, University of Bristol, Dorothy Hodgkin Building, Whitson Street, BS1 3NY Bristol, United Kingdom*

ABSTRACT

Mutations in the thyroid hormone transporter monocarboxylate transporter 8 (MCT8) lead to profound brain alterations, including myelination impairments, in humans. We aimed to further explore the pathophysiological mechanisms underlying the MCT8 deficiency-associated myelination impairments to unravel new biomarkers and therapeutic targets. We have performed brain histological analysis on an MCT8-deficient subject and histological, ultrastructural, and magnetic resonance imaging (MRI) analysis in the brain of a mouse model of the syndrome, lacking MCT8 and enzyme deiodinase type 2 (DIO2, *Mct8/Dio2* KO). We have found that the MCT8-deficient subject presents severely reduced myelin lipid and protein staining and increased proportion of small-caliber myelinated axons in detriment of large-caliber ones. *Mct8/Dio2* KO mice present myelination impairments and abnormal oligodendroglial development. We conclude that the greater proportion of small-caliber axons and impairments in the oligodendroglia lineage progression arise as potential mechanisms underlying the permanent myelination defects in MCT8-deficiency. Moreover, we present the *Mct8/Dio2* KO mouse model, and MRI as a non-invasive biomarker, as highly valuable tools for preclinical studies involving MCT8 deficiency. These findings contribute to the understanding of the pathological mechanisms in MCT8 deficiency and suggest new biomarkers and therapeutic targets to consider therapeutic options for the neurological defects in patients.

1. Introduction

Thyroid hormones (THs), T3 (3,5,3′-triiodo-L-thyronine) and T4 (3,5,3′,5′-tetraiodo-L-thyronine or thyroxine) play an essential role in the developing CNS (Bernal, 2005). While THs are synthesized in the thyroid gland and secreted mostly as T4, the transcriptionally active form is T3 (Cheng et al., 2010). T4 is then converted into T3 in the target tissues by the action of the enzymes deiodinase type 2 (DIO2) and type 1 (DIO1). A crucial step for TH action in the brain is the transport of THs across the brain barriers and the plasma membrane of target cells (Bernal et al., 2015). Among all the transmembrane proteins that can transport THs, the monocarboxylate transporter 8 (MCT8) stands out for its physiological relevance as it presents the highest specificity for the transport of THs (Friesema et al., 2003) and its function is crucial at

human brain barriers (Ceballos et al., 2009; López-Espíndola et al., 2019). Mutations in this transporter lead to the Allan-Herndon-Dudley syndrome (AHDS) or MCT8 deficiency (Allan et al., 1944; Dumitrescu et al., 2004; Friesema et al., 2004), which is a rare X-linked syndrome characterized by severe psychomotor disability and global developmental delay. AHDS is an orphan disease as currently there is no effective treatment for the neurological symptoms of the patients (Grijota-Martínez et al., 2020). MCT8-deficient patients have profound intellectual disability (IQ < 30), speech difficulties, as well as central hypotonia, spastic paraplegia, and dystonic movements. One of the main hallmarks of AHDS is myelination impairments, as most patients have been diagnosed with abnormal white matter (WM) content in different early life stages (for a review, see Vancamp et al., 2020).

Myelination consists of a network of finely regulated processes to

---

insulate axons and enable rapid saltatory conduction of action potentials, facilitating fast communication across neural systems and networks, which is crucial for motor-sensory function and cognition (Saab and Nave, 2017). Importantly, myelination is dependent on TH levels (Calzà et al., 2015), as deficiencies in THs during development result in altered myelin gene expression, impaired oligodendrocyte cell-cycle and consequently in defective myelination (Baas et al., 1997; Bernal, 2005; Valcana et al., 1975; Younes-Rapozo et al., 2006). Oligodendrocytes (OLs), which are glial cells responsible for myelination (Kim and Petratos, 2019), result from the differentiation of oligodendrocyte precursor cells (OPCs) and THs act as a potent differentiation cue during this maturation process (Baas et al., 1997). As myelination is dependent on TH action, is greatly affected in MCT8 deficiency and most patients show abnormal WM content during the first years after birth (Gika et al., 2018; Kobayashi et al., 2014; La Piana et al., 2015; Papadimitriou et al., 2007; Remerand et al., 2019). However, even though myelination defects have been largely known as a hallmark of the disease, the pathophysiological mechanisms behind this feature are still widely unknown. Filling this lack of knowledge would aid better characterization of the syndrome and would contribute to the search of new therapeutic targets and biomarkers to evaluate the outcome of new therapeutic options in preclinical trials.

To this aim, in the present study we have further characterized the myelination phenotype observed by López-Espíndola et al. in 2014 in a MCT8-deficient patient. We have also studied potential alterations in myelination and oligodendroglial lineage in a well-stablished mice model of the disease lacking both MCT8 and DIO2 (*Mct8/Dio2* KO) (Bárez-López et al., 2019), as *Mct8* KO mice faithfully replicate the endocrine symptoms of AHDS but do not present gross neurological abnormalities due the existence of compensatory mechanisms in mice involving DIO2. In this study we have observed persistent myelination impairments in the MCT8-deficient patient, and important alterations in axonal caliber. Moreover, the *Mct8/Dio2* KO mouse model has allowed to describe abnormalities in oligodendroglial development *in vivo*, which, in combination with the alterations in the axonal caliber, are potential mechanisms underlying the myelination defects in MCT8 deficiency. These results represent a step forward in the study of AHDS to date, contributing to the understanding of the pathological mechanisms in MCT8 deficiency and uncovering therapeutic targets and biomarkers, including non-invasive ones, to consider possible treatments for the neurological defects in patients.

2. Materials and methods

2.1. Human samples

Brain tissues were obtained at autopsy from a MCT8-deficient subject and closely age-matched control subjects without known brain pathology.

An 11-year-old boy with MCT8 gene mutation (Q96X) that suffered from severe psychomotor developmental delay, seizures and characteristic thyroid test abnormalities was analyzed in this study. Magnetic resonance imaging (MRI) scan at 9 months of age was within normal limits except for mildly delayed myelination, characteristic of 5 to 6 months of age. A second MRI at age 6.5 years showed mild dilatation of the frontal horns of the lateral ventricles, but no other intracranial abnormality. The child died of respiratory failure secondary to aspiration pneumonia. The tissue blocks were provided by the Sydney Children's and Prince of Wales Hospitals, Randwick, Australia. The following somatic parameters were obtained at autopsy: body weight 29.9 kg; body length approximately 151 cm, brain weight 1285.5 g, cerebral hemispheres weight 1100 g; cerebellum weight 127 g; brainstem weight 25 g.

A 10-year-old girl who died as a result of acute pulmonary oedema during preparation for bone marrow transplant and a 12-year-old boy who died as a result of a diffuse lymphocytic myocarditis were analyzed as control subjects. Paraffin blocks were provided by the Biobank IdiPAZ

(PT20/00004), and L'Hospital Infantil Sant Joan de Déu Biobank, respectively. Tissue blocks were fixed in formalin and embedded in paraffin using standard procedures. Seven μm thin sections were obtained in a microtome (Microm, HM 310) and adhered to glass slides pre-treated with Poly-L-Lysine solution (Sigma-Aldrich, P8920).

2.2. Animal model

Animals were housed in light- and temperature- controlled conditions at $22 \pm 2\,°C$ on a 12:12 light–dark cycle (lights on at 7 AM), with *ad libitum* food and water access. In all experiments, WT and $Mct8^{-/y}/Dio2^{-/-}$ (*Mct8/Dio2* KO) mice were compared. As MCT8-deficiency is an X-linked syndrome, studies in mice were performed in males. *Mct8/Dio2* KO mice were obtained as described in Bárez-López et al. (2019). All genotypes were confirmed by tail DNA PCR as described in Ceballos et al. (2009). Histological experiments were performed in P21, P90 and P180 mice and MRI studies were conducted in P90 and P180 mice.

For histological procedures, mice were anesthetized with ketamine (75 μg/g of body weight) and medetomidine hydrochloride (1 μg/g of body weight), and transcardially perfused with 4% paraformaldehyde in 0.1 M phosphate buffer pH 7.2–7.4 (PB). Brains were removed, postfixed overnight in 4% paraformaldehyde in 0.1 M PB, cryoprotected in 30% sucrose and cut into 30 μm free-floating coronal sections on a cryostat.

For transmission electron microscopy (TEM) procedures, mice were anesthetized with ketamine (75 μg/g of body weight) and medetomidine hydrochloride (1 μg/g of body weight), and transcardially perfused with 2% paraformaldehyde and 2% glutaraldehyde in 0.1 M PB. Brains were removed and postfixed overnight in 2% paraformaldehyde and 2% glutaraldehyde in 0.1 M PB at 4 °C, then conserved in 0.05% sodium azide in 0.1 M PB at 4 °C and finally cut into 100 μm sagittal sections on a vibratome.

2.3. Immunohistochemistry (IHC)

2.3.1. Human samples

Immunohistochemical procedures were the same for the antibodies Myelin Basic Protein (MBP; 1:1000, Abcam ab24567), Myelin Oligodendroglial Glycoprotein (MOG; 1:1000, Abcam ab109746), Proteolipid Protein (PLP; 1:1000, Abcam, Ab9311) and the 70 kDa Neurofilament (NEFL; ready to use, Dako IS607). To avoid methodological differences, tissue from control and MCT8-deficient subjects were processed in parallel. Moreover, specificity of the secondary antibodies was validated for each experiment using negative controls without primary antibodies. Sections were deparaffinized in xylene and hydrated in decreasing ethanol concentrations. Following dewaxing and hydration, tissue sections were subjected to an antigen retrieval process with EnVision FLEX High pH (Dako, K8004) solution at 95 °C for 20 min. Endogenous peroxidase was blocked for 15 min with 3% hydrogen peroxide in distilled water at room temperature (RT) in dark. In order to reduce the nonspecific binding for the antibodies, samples were incubated in a blocking solution containing 4% BSA (Sigma, A4503), 0.1% Triton X-100 in PBS pH 7.2–7.4) with 5% of serum (Vector Laboratories, S-1000), for 1 h. Sections were incubated overnight at 4 °C with primary antibodies in 4% BSA, 0.1% Triton X-100 and 1% serum. Tissues were incubated with biotinylated secondary antibodies at 1:200 concentration in 4% BSA, 0.1% Triton X-100 and 1% serum at RT for 1 h. For signal amplification, the sections were incubated with Avidin-Biotin Complex (ABC Elite Kit Vector Laboratories, #32050) in dark at RT for 1 h and developed with 0.5 mg/mL diaminobenzidine (Sigma, D5637) and 0.01% hydrogen peroxide. Finally, sections were dehydrated in ascending ethanol concentrations, cleared in xylenes, and covered with hydrophobic mounting medium Depex (Serva, 18243).

2.3.2. Mice samples

The same protocol was followed for the following antibodies platelet-

derived growth factor receptor-alpha (PDGFRα: 1:250, R&D, AF1062), oligodendrocyte transcription factor 2 (OLIG2; 1:250, Calbiochem, AB9610), and adenomatous polyposis coli clone CC1, for mature oligodendrocytes (CC1; 1:100, Millipore, OP80). For MBP (1:1000, Abcam ab24567) an additional step was added, as slices were incubated for 15 min in cold methanol (kept at −20 °C) prior to incubation in blocking solution. WT mice and *Mct8/Dio2* KO mice tissues were processed in parallel. Endogenous peroxidase for free-floating mice sections was blocked by incubating in dark with 3% hydrogen peroxide and 10% methanol in PBS at RT for 15 min, and no antigen retrieval was performed. Nonspecific antibody binding was prevented by blocking with 4% BSA, 0.1% Triton X-100, 0.1 M Lysin and 5% serum at RT for 1 h. Incubation with primary and secondary antibodies, signal amplification and development were the same as described above for human tissues.

Analysis of myelin status was performed in both human and mice samples immunolabeled with MBP. In mice, 30 μm tissue sections from the forebrain at Bregma 1.10, 0.86, 0.62, 0.38, and 0.14 were used for each animal at all the studied timepoints. Secondary motor cortex of both hemispheres was captured at 10× magnification (Numerical aperture 0.30) with a Nikon Eclipse 80i microscope and a Nikon DSFi1 digital camera. By means of NIH Image J® software (Wayne Rasband, National Institutes of Health), both the percentage of area occupied by the immunolabelling as well as the intensity of the immunoreaction (mean gray value) were recorded for each photograph and used to calculate the AI index (% area immunolabeled multiplied by the mean gray value) as described by Almolda et al. (2014). For the quantification of MBP immunolabelling intensity in the corpus callosum (cc), three 10× magnification images were captured covering all the cc structure for each tissue section. Each tissue section was assigned a value calculated as the average of three identical regions of interest (ROIs), placed one on each cc knee and one at the midline of the cc. cc thickness was measured at the midline of each section by Image J®.

For human samples, given that only one subject per condition was available, 5 random images were captured at 10× magnification in both subjects for each cortical layer of the motor cortex, and the AI index was calculated for the entire image as described above. The analysis and delimitation of the cortical layers in the human CNS was done based on the axonal disposition in the MBP immunopositive tissue sections and using an adjacent tissue section stained with Luxol Fast Blue (LFB) counterstained with 10% cresyl acetate (Klüver-Barrera's stain) to stain neural cell bodies as well as myelin sheaths. Layer I was easily delimited due to its enrichment in horizontal myelinated fibers, that can be associated with thalamo-cortical matrix-type axons. Layers II and III present a much lower abundance of axonal tracts as compared to layers I and IV. In layer IV or internal granular layer, both horizontal (cortico-cortical) and vertical (thalamo-cortical) fibers can be found, where thalamo-cortical fibers tend to aggregate around the granular neurons characteristic of this layer. In layer V, pyramidal tract neurons can be found, along with their projection of axonal tracts towards subcortical structures such as basal ganglia or towards intratelencephalic neurons. Finally, layer VI spans from the lower limit of layer V to the transition zone towards the subcortical white matter.

Quantification of oligodendroglial lineage cells was performed in the anterior commissure (ac) using at least three animals for each genotype at each studied timepoint (P21, P90, P180). For each animal, brain sections were stained for CC1, PDGFRα, and OLIG2 and all the immunopositive cells in the ac were counted along the whole *Z*-axis using a 100× oil-immersion objective (Numerical aperture 1.30). Images for the all the oligodendroglial markers were taken at the ac using a 40× objective (Numerical aperture 0.75).

2.4. Histological staining

2.4.1. Sudan Black B (SBB) staining

Sections were hydrated in progressively decreasing ethanol concentrations up to 70% and then incubated in 0.5% SBB (Fluka, 86015)

70% ethanol for 30 min. Finally, samples were rinsed in 70% ethanol and rehydrated progressively before covering them in in hydrophilic mounting medium (8% gelatin, 50% glycerin in distilled water).

2.4.2. LFB staining

LFB was performed following the manufacturer's protocol (Electron Microscopy Sciences, 26681).

In human samples the diameter of well-defined myelinated axons was measured in several axonal tracts (cerebral peduncle, medial lemniscus, superior cerebellar peduncle, medial longitudinal fasciculus) of pons and midbrain sections from control and MCT8-deficient subjects using the LFB technique. Transverse cuts present in 3 random fields of 0.01 mm^2 each, at a 100× magnification, were measured using Nikon NIS software. Measurements were made from one side to the opposite of the outer edges of the myelin sheath. In cases where the sheath shape was elongated and not rounded, the smaller diameter was measured.

Images for both IHC and histological staining were obtained with a Nikon Eclipse 80i microscope and a Nikon DSFi1 digital camera.

2.5. Transmission electron microscopy (TEM)

Mice brain slices were postfixed in 2% OsO$_4$ in 0.1 M PB (90 min at RT) and 2% uranyl acetate stained (150 min at 4 °C in the dark), ethanol dehydrated, immersed in propylene oxide (Lab Baker, Deventry, Holland) and embedded overnight in Araldite (Durcupan, Fluka, Buchs SG, Switzerland). Ultrathin sagittal sections (60 nm) of the cc genu were obtained using an ultramicrotome (Leica Ultracut S, Leica, Heidelberg, Germany) then put on 200 mesh copper grids and counterstained with lead citrate.

Images were then obtained with a transmission electron microscope Jeol Jem1010 (Jeol, Tokyo-Japan) equipped with a Gatan SC200 digital camera (Gatan Inc., Pleasanton, CA).

For quantitation of myelin thickness and G ratio in mice samples, axon and fiber diameter were measured in 10 random axons per field (at least 5 fields per animal) using Image J®. Myelin thickness was calculated as (fiber diameter-axon diameter)/2, and G ratio was calculated as (axon diameter)/(fiber diameter). Percentage of myelinated axons was calculated for each animal as the average of (number of myelinated axons)/(myelinated + non-myelinated axons) for each field.

2.6. MRI experiments

MRI experiments were performed on a Bruker Pharmascan system (Bruker Medical Gmbh, Ettlingen, Germany) using a 7.0-T horizontal-bore superconducting magnet equipped with a ^{1}H selective birdcage resonator of 23 mm and a Bruker gradient insert with 90 mm of diameter (maximum intensity 36 G/cm). All data were acquired using a Hewlett-Packard console running Paravision 5.1 software (Bruker Medical Gmbh) operating on a Linux platform. Mice were anesthetized with a 2% isoflurane in 1 L of oxygen in an induction chamber. Animal temperature was maintained approximately at 37 °C. The physiological state of the animals was monitored using an MRI compatible small animal gating system by SA Instruments (Stony Brook, NY) that controlled the respiratory rate. Diffusion tensor imaging (DTI) data were acquired with a spin echo single shot echo planar imaging (EPI) pulse sequence using the following parameters: TR/TE 3500/40 ms; a signal average of 4.7, noncollinear diffusion gradient scheme with a diffusion weighting b = 110 and 1400 s/mm^2, slices thickness 1 mm without a gap, field of view 23 × 23 mm and acquisition matrix = 128 × 128. Fractional anisotropy, mean diffusivity, trace, the eigenvalues and eigenvector maps were calculated with a homemade software application written in Matlab (R2007a). The captured images were analyzed using Image J, that calculates the mean value for all pixels contained in the selected brain region. T2-weighted (T2-W) spin-echo images were acquired with a rapid acquisition with relaxation enhancement (RARE) sequence in axial orientations. The following parameters were used: TR = 2500 ms, TE =

44.3 ms, RARE factor = 8, Av = 3, FOV = 2.3 cm, acquisition matrix = 256 × 256 corresponding to an in-plane resolution of 90 × 90 m², slice thickness = 1.00 mm without gap and number of slices = 14.

2.7. Statistics

Data were expressed as mean ± SEM. Statistical analyses were performed with GraphPad Software (www.graphpad.com). Assessment of the normality of data was performed by Shapiro-Wilk test. Means between two groups were compared by 2-tailed, unpaired Student's *t*-test for parametric data or by Mann-Whitney test for non-parametric data. Differences between means for more than two groups was performed by Kruskal-Wallis test for non-parametric data. Significant differences were represented as $*P < 0.05$; $**P < 0.01$, and $***P < 0.001$.

2.8. Ethics statement

2.8.1. Human studies

Tissue samples were collected and processed following standard operating procedures with the appropriate approval of the Ethics and Scientific Committees (Consejo Superior de Investigaciones Científicas, CSIC, permit number SAF2017-86342-R) and with written informed consent from the parents of all subjects, in agreement with the Declaration of Helsinki. The smallest possible number of samples was used to perform these studies and all personal data were treated anonymously.

2.8.2. Animal studies

All experimental procedures involving animals were performed following the European Union Council guidelines (directive 2010/63/UE) and Spanish regulations (R.D. 53/2013) and were approved by the ethics committee Comité de Ética y Experimentación Humana y Animal (CEEHA) at CSIC and by the Comunidad Autónoma de Madrid Review Board (proex 162/17) for the use of animals for scientific purposes.

3. Results

3.1. Persistent myelination impairments in the MCT8-deficient brain

In order to study the myelin status in MCT8 deficiency we have analyzed different myelin lipid and protein components. To assess the lipid component, histological stainings were performed with SBB and LFB. For the protein component, IHC was used to study MBP, MOG, and PLP.

The study of the lipids revealed paler lipid staining by both SBB and LFB in the WM of the cerebellum (Fig. 1) and the internal capsule (Supplementary Fig. 1) of the 11-year-old MCT8-deficient subject compared to the control. Similar results were found regarding proteins, as MOG and PLP stainings revealed lower myelin protein signal in the cerebellar WM of the MCT8-deficient patient in comparison to the control (Fig. 1). The same pattern was observed in myelin-related proteins in the motor cortex (Fig. 2) and the internal capsule (Supplementary Fig. 1). Moreover, when studied at greater magnification, the MCT8-deficient WM showed a lower density of myelin sheaths compared to the control subjects in all regions studied, as shown for the cerebellum and motor cortex (Fig. 1k,l,o,p and Fig. 2i,j).

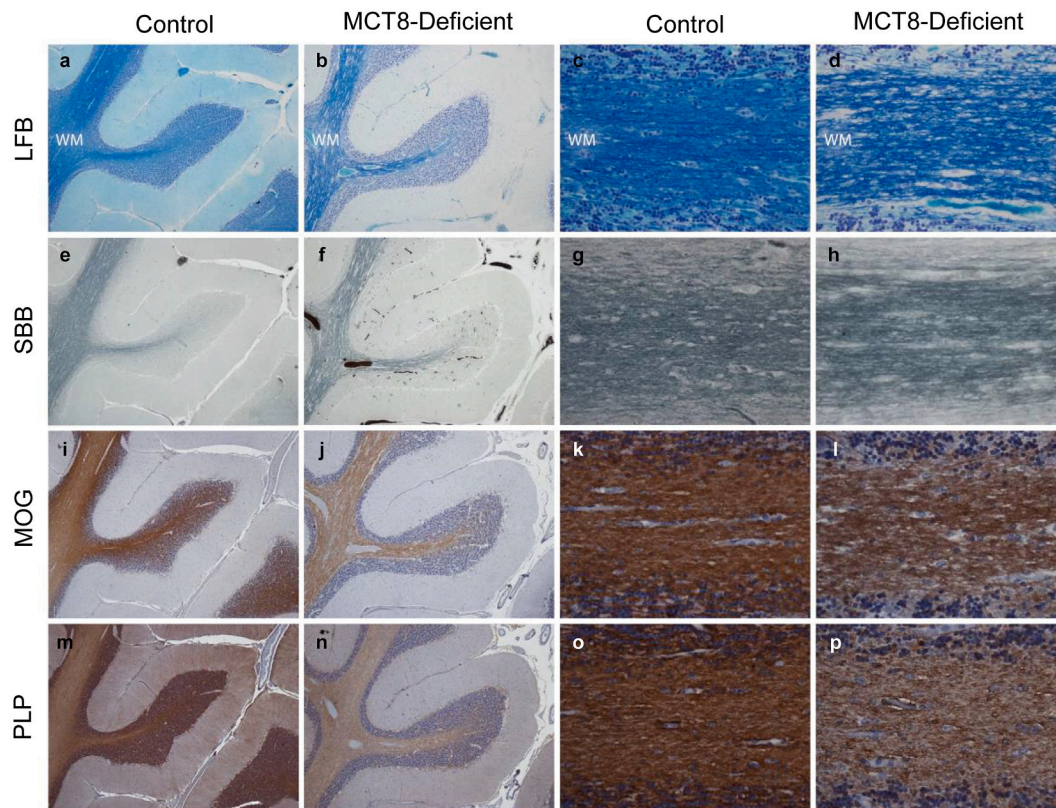Regarding MBP immunostaining, the MCT8-deficient subject

Fig. 1. Cerebellar myelination impairments in an 11-year-old MCT8-deficient subject. Representative images showing LFB (a-d) and SBB (e-h) lipid staining and myelin protein immunostaining for MOG (i-l) and PLP (m-p) in tissue sections of the cerebellar vermis from control (a, c, e, g, i, k, m, o) and MCT8-deficient (b, d, f, h, j, l, n, p) child. Note the lower intensity staining (a, b, e, f, i, j, m, n) and lower density of myelin sheaths (c, d, g, h, k, l, o, p) in the cerebellum of the MCT8-deficient boy as compared to the 10-year-old control subject. Scale bars represent 1100 μm (a, b, e, f, i, j, m, n) and 110 μm (c, d, g, h, k, l, o, p). LFB: Luxol Fast Blue; MOG: Myelin Oligodendrocyte Glycoprotein; PLP: Proteolipid Protein; SBB: Sudan Black B. (For interpretation of the references to colour in this figure legend, the reader is referred to the web version of this article.)
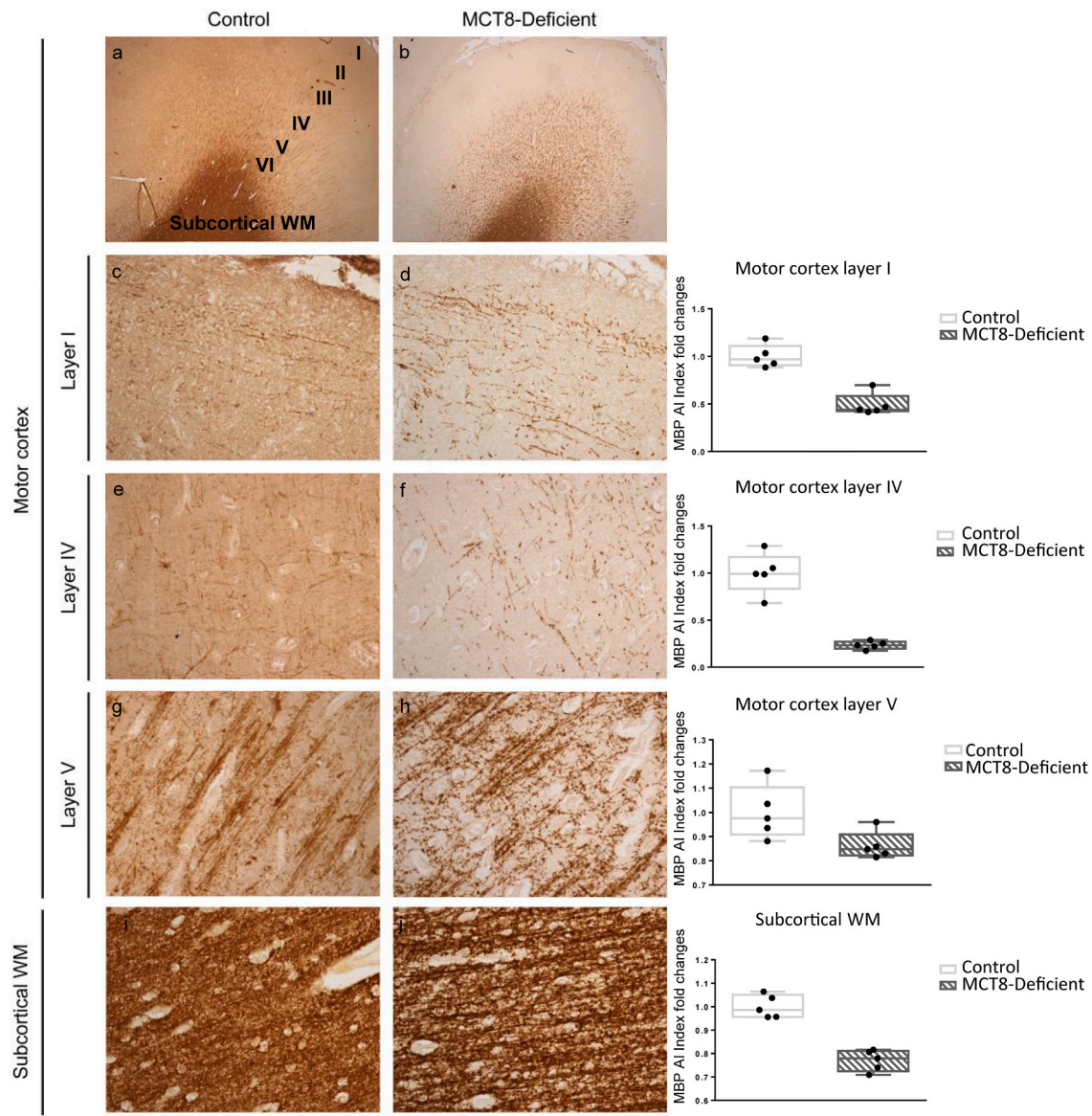
Fig. 2. Expression of MBP in the human motor cortex. Representative images showing expression of MBP in the motor cortex and subcortical WM from a control and a MCT8-deficient child. I, II, III, IV, V and VI represent the different layers of the cerebral cortex. Scale bar represents 1540 μm in a, b; and 77 μm in c-j. Each graph depicts fold changes in the AI index for the cortical layer to its left in the MCT8-deficient child as compared to the 12-year-old control subject. Data are shown as box and whiskers plots (min to max). MBP: Myelin Basic Protein; WM: White Matter.

presented an overall reduction in comparison to the control in all the studied layers of the motor cortex (layer I, IV, V 51%, 77%, 14% reduction, respectively; Fig. 2), as well as in the subcortical WM (23% reduction; Fig. 2). In addition, the evaluation of the motor cortex of the MCT8-deficient subject revealed a disorganization of the myelinated tracts in layer V, compared to the control, as well as a decrease in the density of myelinated fibers in the subcortical WM (Fig. 2).

3.2. Lower proportion of large caliber axons in several myelinated tracts

The caliber of myelinated axons in the MCT8-deficient subject brain was studied using the LFB technique and immunostaining against NEFL in different regions of the brainstem (Fig. 3 and Fig. 4). In the cortico-spinal tract of the cerebral peduncle (Fig. 4a), the average caliber size was 2.12 ± 1.10 μm in the control subject, and much lower in the MCT8-deficient boy (1.51 ± 0.79 μm). Moreover, the corticospinal tract in the cerebral peduncle of the MCT8-deficient patient consisted mainly of small (less than 3 μm in diameter) caliber myelinated axons in detriment

of medium-size ones (3–6 μm in diameter) and, in contrast to the control sample, no large (more than 6 μm in diameter) caliber myelinated axons could be detected. At the medial lemniscus (Fig. 4b), the average caliber size was 2.7 ± 1.24 μm for the control subject and 1.76 ± 0.88 μm in the MCT8-deficient patient. Similar findings were observed in the superior cerebral peduncle (Fig. 4c) and the medial longitudinal fasciculus (Fig. 4d) where the average myelinated axonal diameter was much lower in the MCT8-deficient patient, as control values were 3.22 ± 1.75 μm and 2.71 ± 1.62 μm in the superior cerebral peduncle and the medial longitudinal fasciculus, respectively, and 1.98 ± 0.79 μm and 2.12 ± 0.84 μm in the MCT8-deficient patient. As for the corticospinal tract, the proportion of small caliber axons increased in detriment of medium-size and large caliber myelinated axons in the medial lemniscus, the superior cerebral peduncle and the medial longitudinal fasciculus of the MCT8-deficient subject, where no large caliber myelinated axons could be detected in contrast to the control sample (Fig. 3 and Fig. 4). Interest-ingly, the morphological features of the myelin sheaths of myelinated axons in the MCT8-deficient patient did not differ qualitatively from
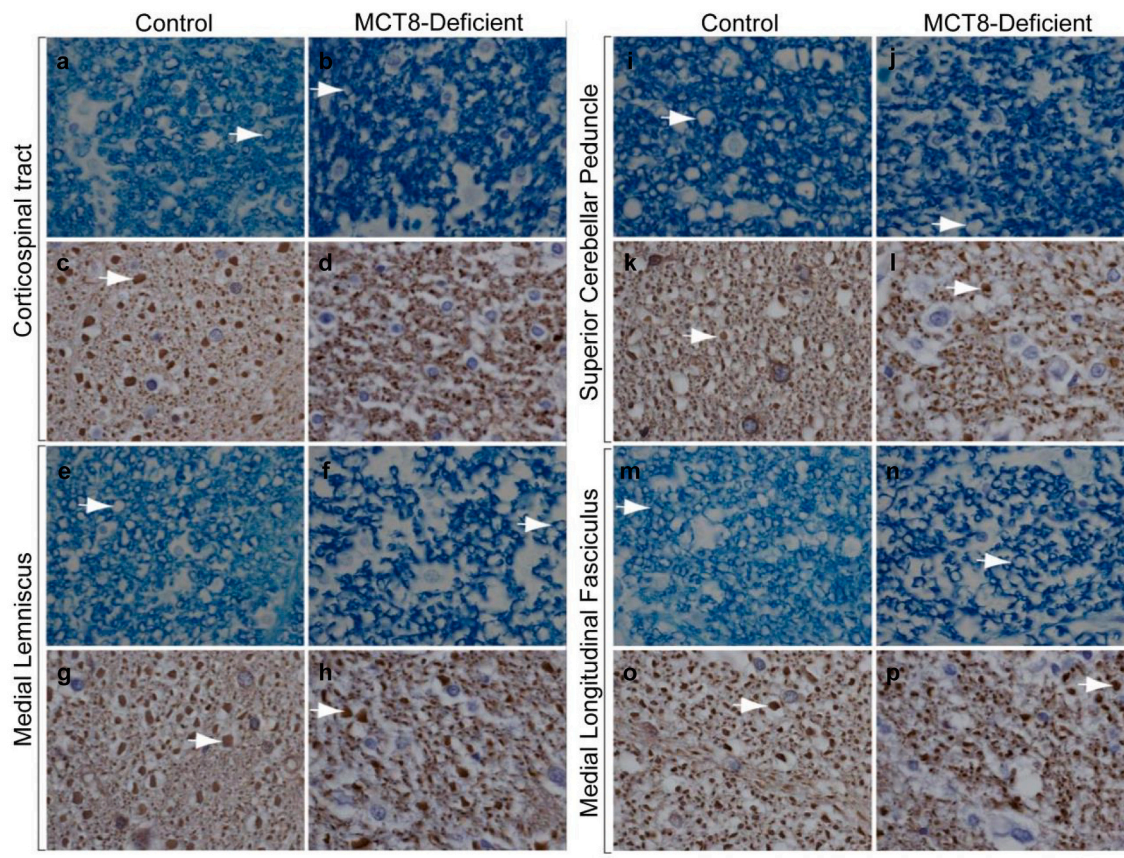
Fig. 3. Axon calibers as depicted by LFB and NEFL. Representative images showing LFB lipid staining (a, b, e, f, i, j, m, n) and NEFL immunostaining (c, d, g, h, k, l, o, p) in tissue sections of the brainstem at the corticospinal tract (a-d), the medial lemniscus (e-h), the superior cerebellar peduncle (i-l) and the medial longitudinal fasciculus (m-p) of control and MCT8-deficient children. Control samples correspond to the 10-year-old subject. Arrows point to some examples of large axons mainly found in the control subject. Note the low proportion of high caliber axons in the MCT8-deficient child. Scale bar represents 22 μm. LFB: Luxol Fast Blue; NEFL: 70 kDa neurofilament. (For interpretation of the references to colour in this figure legend, the reader is referred to the web version of this article.)

control samples (Fig. 3).

Similar results were obtained by analyzing the axonal diameter of axons immunostained with antibodies against the NEFL protein further supporting that, in the MCT8-deficient subject, all the studied axonal tracts are mostly composed of small caliber axons (Fig. 3).

3.3. Reduced myelination in the Mct8/Dio2 KO mice brain: histological studies

In order to assess possible abnormalities on WM formation and development on an animal model of MCT8 deficiency, coronal sections of *Mct8/Dio2* KO and wild type (WT) mice brains were immunostained against MBP at different developmental stages. Staining intensities were visibly lower in the secondary motor cortex (46.5% reduction), as well as in WM areas such as the cc (24.5% reduction) (Fig. 5a,b) of *Mct8/Dio2* KO mice compared to WT animals at Postnatal day 21 (P21). Not only the intensity of the staining was lower but a significant reduction in cc size was also quantified in *Mct8/Dio2* KO animals in comparison to WT (Fig. 5c). Moreover, in addition to the paler staining, axonal tracts in the caudate nucleus (Supplementary Fig. 2) were less defined in *Mct8/Dio2* KO tissue samples as a sign of lower density of myelin sheaths.

With aging, some of these abnormalities appear to mitigate as, at P90, the differences in MBP immunostaining intensity values between *Mct8/Dio2* KO and WT mice were less pronounced. *Mct8/Dio2* KO mice displayed a 33.65% reduction in MBP staining intensity values in secondary motor cortex and a 23.1% reduction in the cc (NS) in comparison to WT levels (Fig. 5a,b). In addition, cc size (Fig. 5c) and definition of axonal tracts in the caudate nucleus (Supplementary Fig. 2) were also

more similar to WT samples, although none of them fully recovered. Finally, at P180, *Mct8/Dio2* KO mice showed a bigger extent of recovery. While MBP immunostaining intensity (Fig. 5a,b) and cc size (Fig. 5c) were not statistically significant different from WT values, at a qualitative level the lack of definition of the big axonal tracts and the presence of non-grouped myelinated fibers in the caudate nucleus of *Mct8/Dio2* KO mice suggested structural myelination impairments at this age (Supplementary Fig. 2).

3.4. Reduced myelination in the Mct8/Dio2 KO mice brain: MRI studies

DTI, commonly used to evaluate microstructural variations in brain tissue, was used to study the myelin status in the *Mct8/Dio2* KO mice brain. Data were obtained for three parameters: 1) Fractional Anisotropy (FA), which increases in presence of parallel myelinated axons; 2) Axial Diffusivity (AD), which is widely considered as a marker of axonal integrity; and 3) Radial Diffusivity (RD), which values increase with reduced myelin density (Sun et al., 2017; Yano et al., 2018).

DTI data were obtained from WT and *Mct8/Dio2* KO mice at P90 and P180, and FA, AD, and RD values were calculated in all animals for a ROI delimitating the cc (Fig. 6). The FA and AD values were significantly lower in *Mct8/Dio2* KO mice at P90, as FA and AD values were 60% and 43.5% lower, respectively, from the values observed in the WT animals, indicating impairments in myelination as well as in axonal integrity (Fig. 6a). RD values were higher in *Mct8/Dio2* KO animals by 38% at P90 indicating a decay on the myelination (Fig. 6a). At P180, differences in FA and AD persisted, as *Mct8/Dio2* KO mice values were, respectively, 58% and 40% lower than those observed in the WT animals (Fig. 6b).
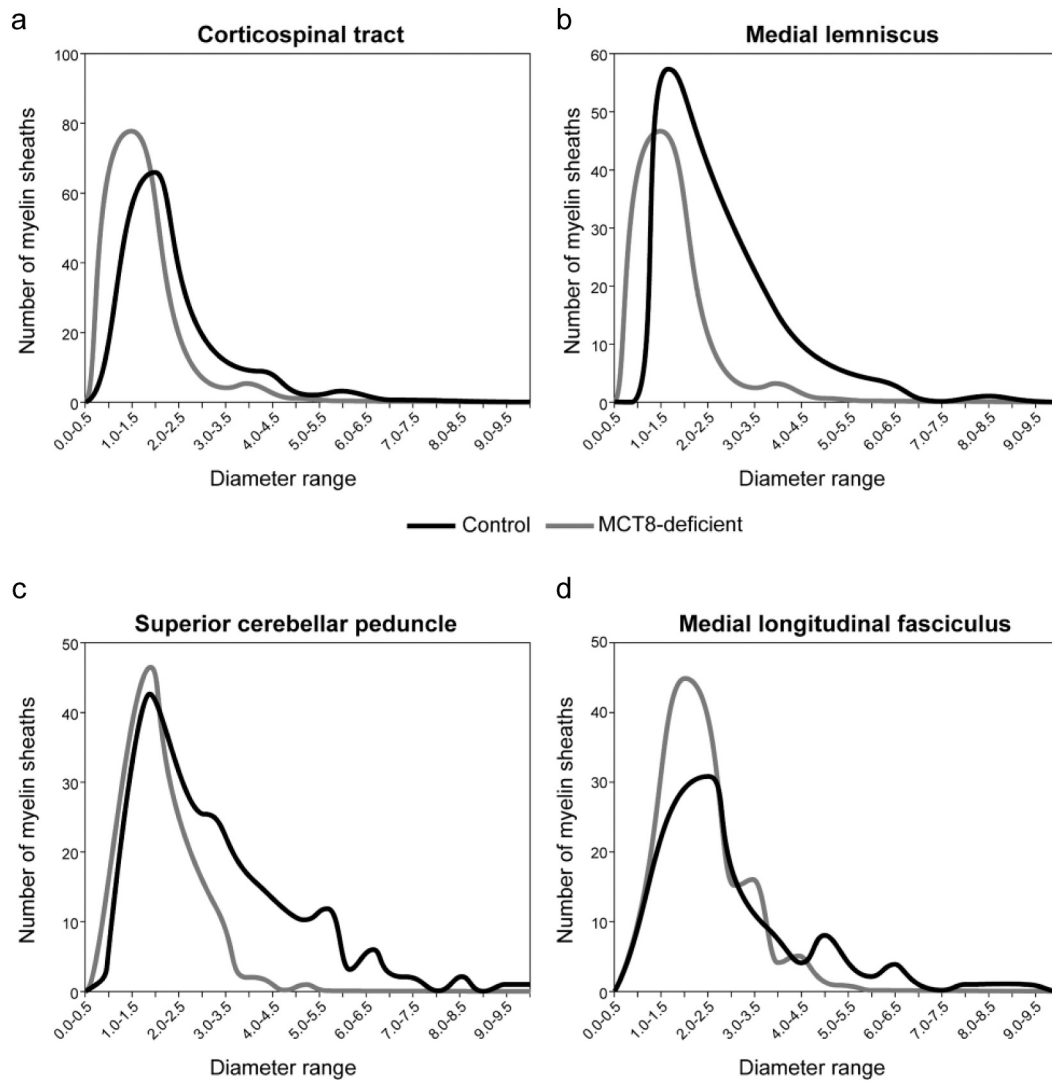
Fig. 4. Graphs describe the distribution of the diameter of myelinated axons of the brainstem at the corticospinal tract (a), medial lemniscus (b), superior cerebellar peduncle (c) and medial longitudinal fasciculus (d) from control (black line) and MCT8-deficient (gray line) children. The diameters of the myelinated axons are expressed in 0.5 μm ranges. Statistical analyses showed significant differences between the control and MCT8-deficient samples in axonal diameter in all tracts ($p <$ 0.0001 for cerebral peduncle, medial lemniscus and superior cerebellar peduncle; and $p = 0.0069$ for medial longitudinal fasciculus were determined by Mann-Whitney test).

However, differences in RD, with *Mct8/Dio2* KO values 23% higher than in WT animals, were non-statistically significant at this age (Fig. 6b).

In summary, MRI studies showed persistent alterations in white matter microstructure.

3.5. Reduced myelination in the Mct8/Dio2 KO mice brain: ultrastructural studies

In order to deepen into the impairments in myelination observed in *Mct8/Dio2* KO mice, ultrastructural studies were carried out by TEM on ultrathin brain sections of *Mct8/Dio2* KO and WT mice at P90 and P180. The WM area chosen for this study was the cc at midline level in sagittal plane (Fig. 7).

Mct8/Dio2 KO mice exhibited widespread patches of non-myelinated axons at both studied timepoints, with less than one third of the total number of axons being myelinated at both P90 (28.92 ± 2.78) and P180 (31.81 ± 2.05). In contrast WT mice showed ubiquitous myelination at P90 and P180 (68.23 ± 1.41 and 65.42 ± 1.88, respectively) (Fig. 7a,b and Supplementary Fig. 3a).

Moreover, the status of the myelin sheaths of the axons was also

elucidated. For this, average myelin thickness and G-ratio were calculated for both WT and *Mct8/Dio2* KO mice at both timepoints, in addition to a qualitative assessment of the myelin sheath integrity. Data obtained revealed no major differences in these parameters between both genotypes (Fig. 7a,c and Supplementary Fig. 3b).

In summary, TEM studies showed a decrease in the number of myelinated axons, however, the axons that were myelinated presented no obvious alterations in myelin integrity.

3.6. Oligodendroglial populations are disrupted in Mct8/Dio2 KO mice

Oligodendroglial populations were studied at different timepoints (P21, P90, and P180) by IHC. Data analysis was conducted in the ac, as this is a TH-influenced WM representative area, which is easy to delimitate (Guadaño-Ferraz et al., 1994).

Antibodies against PDGFRα were used to assess the OPCs population in the *Mct8/Dio2* KO mice. This study showed that OPCs density in WT mice does not change significantly throughout aging from P21 to P180 (Fig. 8a). However, *Mct8/Dio2* KO mice showed a higher OPCs density in comparison to WT animals at P21 that diminished throughout aging, so
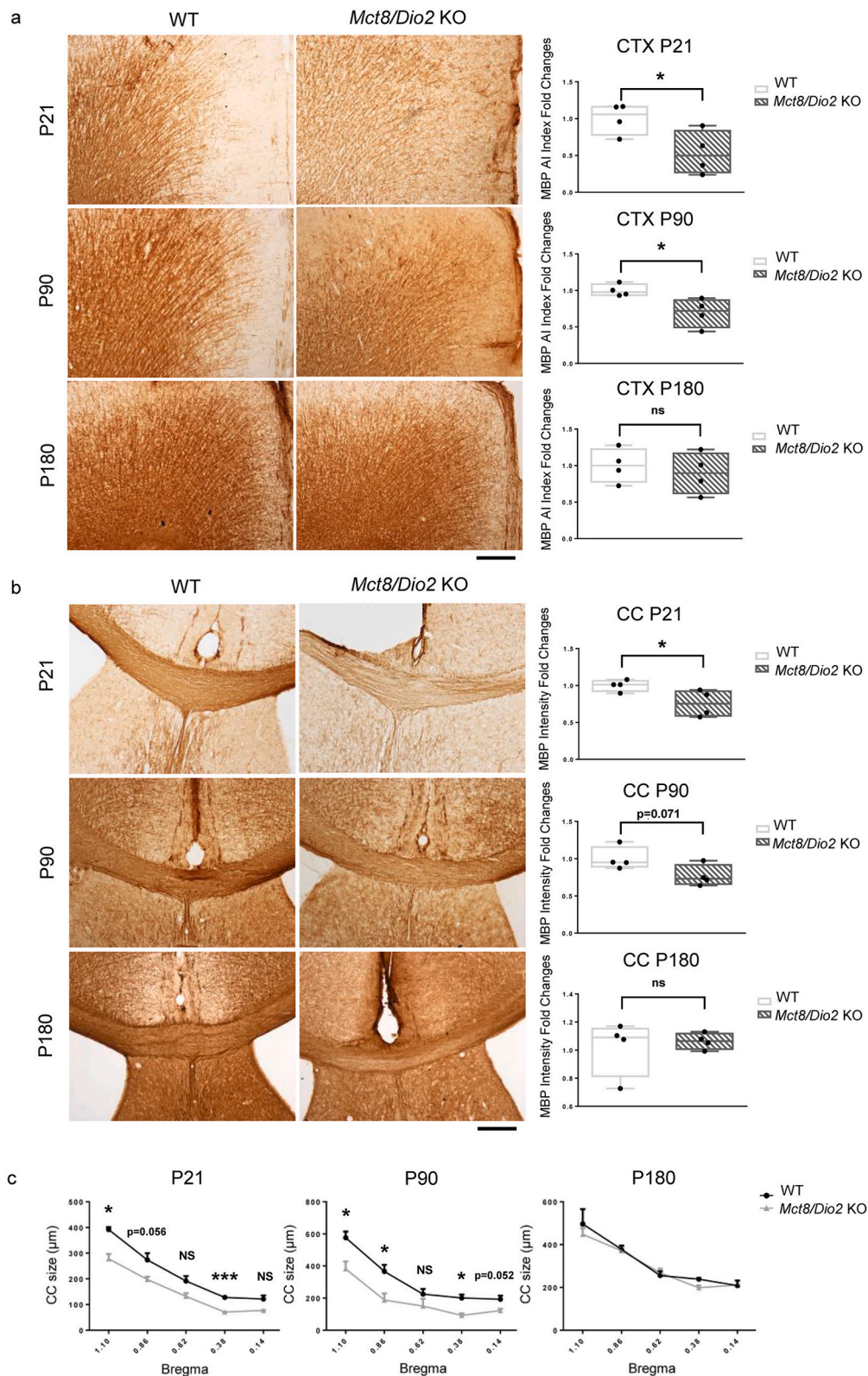
Fig. 5. Histological analyses of the myelination impairments in *Mct8/Dio2* KO mice. Expression of MBP in brain coronal sections of WT (*n* = 4) and *Mct8/Dio2* KO (n = 4) at different developmental stages (P21, P90 and P180). Representative images depict the secondary motor cortex (a) and the corpus callosum (cc; b). P21 *Mct8/ Dio2* KO samples show paler staining for all the studied areas and a reduction in cc size (b). Throughout aging, differences in staining intensity become less pronounced, but are still present. Each graph on a and b depicts fold changes in the AI index for the structure and timepoint to its left in the *Mct8/Dio2* KO as compared to WT animals. cc size was also measured for each of the Bregma points studied, as shown in c. AI Index: % area immunolabeled multiplied by the mean gray value. Data are shown as box and whiskers plots (min to max) in a, b, and mean ± SEM in c. *$p < 0.05$, *p* values were determined by unpaired Student's *t*-test. Scale bars a and b 500 μm, c 125 μm. MBP: Myelin Basic Protein.
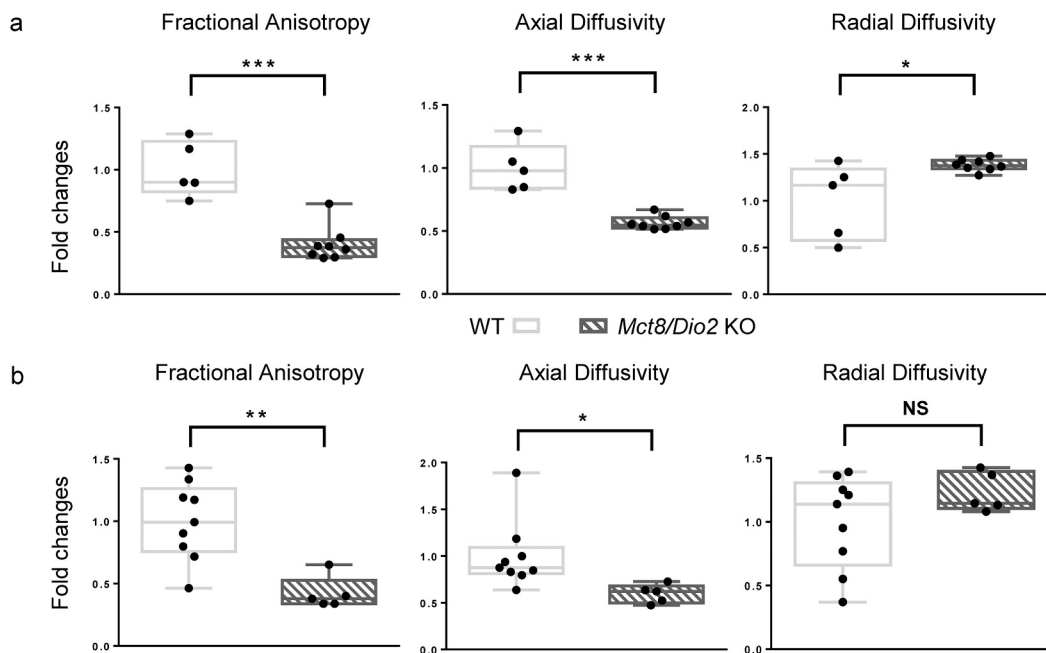
Fig. 6. Magnetic resonance imaging (MRI) diffusion tensor imaging (DTI) parameters in *Mct8/Dio2* KO mice show permanent myelination impairments in the corpus callosum (cc). Graphs show differences, expressed as fold changes, between WT (P90: $n = 5$; P180: $n = 9$) and *Mct8/Dio2* KO (P90: $n = 8$; P180: n = 5) mice for each DTI parameter: fractional anisotropy, axial diffusivity, radial diffusivity; in the cc, at P90 (a) and P180 (b). Data are shown as box and whiskers plots (min to max). *p < 0.05, **$p < 0.01$, ***$p < 0.005$, p values were determined by unpaired Student's t-test.

at P90 and P180 differences in OPCs density could no longer be observed between WT and *Mct8/Dio2* KO animals (Fig. 8a,d). Moreover, examination of higher magnification images revealed abnormalities in OPCs morphology and size in *Mct8/Dio2* KO mice at P21 as *Mct8/Dio2* KO OPCs were larger in size and branching compared to WT mice (Fig. 8a and Supplementary Fig. 4).

In order to study maturation of OLs, staining with anti-CC1 antibody, that labels mature OLs, was carried out. WT animals displayed a high density of CC1 immunopositive (CC1$^+$) cells at P90 that decreased at P180 (Fig. 8b). *Mct8/Dio2* KO mice showed a lower density of mature OLs at P90 in comparison to WT animals (Fig. 8b,e).

Finally, the whole oligodendroglial lineage was assessed with anti-OLIG2 staining. In WT animals, a remarkable increase in oligodendroglial cells density was observed between P21 and P90, which then decreased at P180 (Fig. 8c,f). In *Mct8/Dio2* KO mice, the oligodendroglial cells density at P21 was considerably higher than in WT mice. This difference was inverted at P90, as *Mct8/Dio2* KO mice showed a lower oligodendroglial cells density compared to WT mice. At P180, however, no differences could be appreciated in oligodendroglial cells density between *Mct8/Dio2* KO and WT mice (Fig. 8c, f).

This *in vivo* study provides quantitative statistically significant data indicating that *Mct8/Dio2* KO animals present alterations in oligodendroglial lineage cells.

4. Discussion

Myelination, one of the most crucial stages during brain development, is known to be largely dependent on THs (Gothié et al., 2020). Even though impairments in myelin is one of the main hallmarks of MCT8 deficiency, the underlying mechanism remains poorly understood. In the present study we have explored the myelination impairments in an MCT8-deficient subject and in a model of MCT8 deficiency, *Mct8/Dio2* KO mice, in order to describe the different myelination defects throughout aging and to unravel the causes underlying these impairments.

In order to better characterize the myelin status in MCT8 deficiency,

we have analyzed in more depth several myelin lipid and protein components in several brain regions, as well as the extent of myelination of axons from different tracts in post-mortem cerebral samples of an 11-year-old MCT8-deficient patient. We have found alterations in myelination with decreased phospholipids and glycolipids staining, as well as lower immunostaining of myelin proteins such as MOG, PLP, and MBP in all the brain regions analyzed. Moreover, a detailed study of the myelinated axon diameter in different sensory and motor axonal tracts has revealed a higher proportion of small-caliber axons and significantly lower number of large-caliber myelinated axons in the MCT8-deficient patient. This was observed both by LFB staining and immunostaining for the neurofilament protein NEFL, being the latter consistent with previous findings where we found decreased staining of neurofilament proteins in MCT8-deficient fetal brain tissue (López-Espíndola et al., 2014). In addition, in previous studies we also found paler neurofilament immunostaining in several brain regions of *Mct8/Dio2* KO mice in comparison to WT (Bárez-López et al., 2019). Since neurofilaments regulate axonal diameter and, as axonal diameter is determinant for stimulation of myelination (Friede, 1972; Voyvodic, 1989), these findings raise the possibility that a small axonal diameter might be one of the factors impairing the correct myelination in MCT8 deficiency.

In order to further explore the pathophysiological mechanisms underlying these myelination impairments, we have assessed whether the *Mct8/Dio2* KO mouse reproduces the myelination impairments observed in humans (López-Espíndola et al., 2014). While the *Mct8/Dio2* KO mouse model present its drawbacks as a model for MCT8 deficiency, as it lacks both MCT8 and DIO2 (an essential enzyme for TH metabolism in the brain), it is probably the most suitable mouse model available to date to study the human MCT8 deficiency neurological impairments. *Mct8/Dio2* KO mice resemble the neurocognitive impairments due to MCT8 deficiency, and these arise from knocking out genes encoding proteins solely involved in TH availability and action. (Grijota-Martínez et al., 2020). Histological, TEM and MRI studies showed severe myelin impairments present from early developmental stages that, although improved with age, persisted at later stages. Similar to the observations in human samples (López-Espíndola et al., 2014, and present studies),
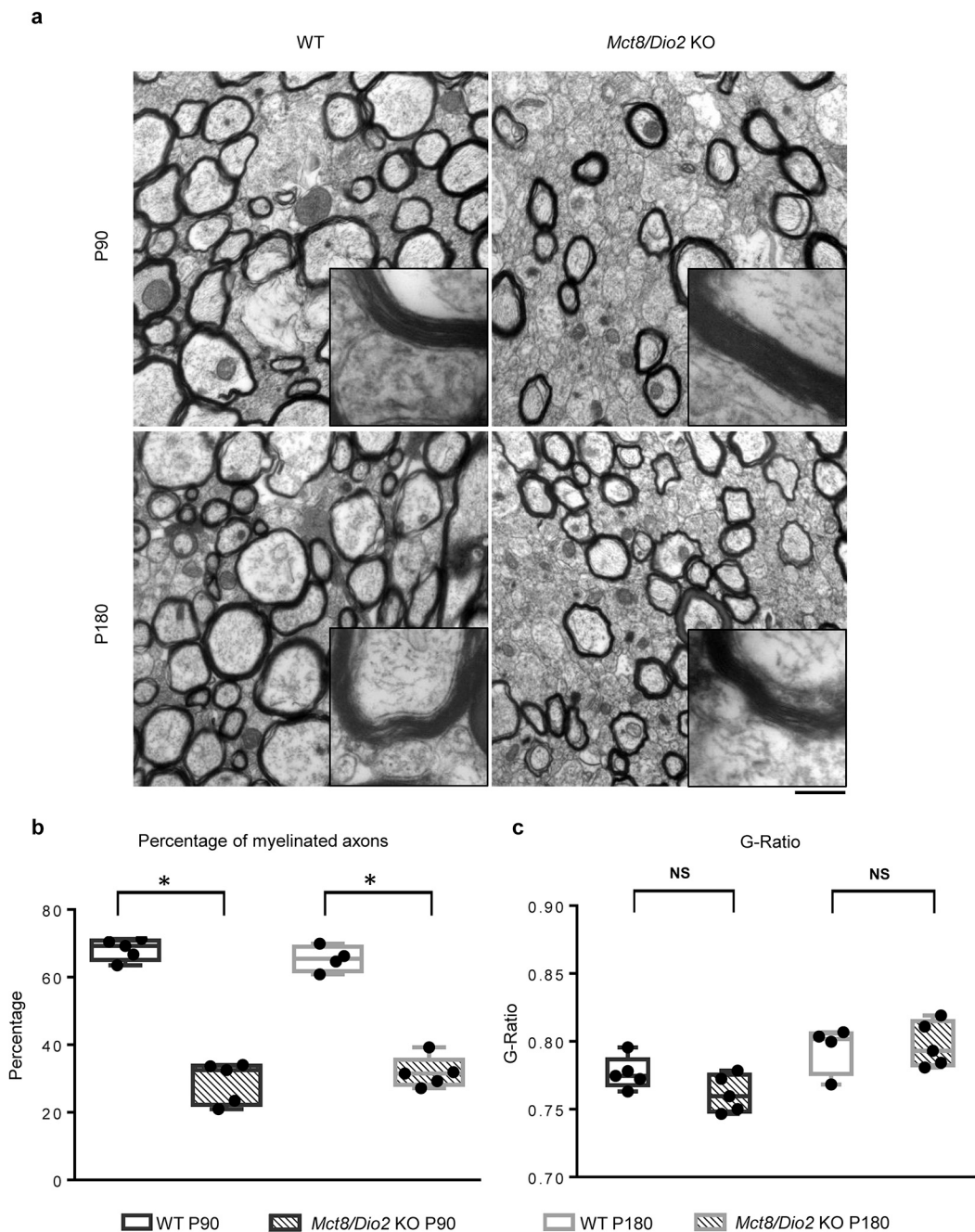
Fig. 7. Altered myelination pattern in *Mct8/Dio2* KO mice. (a) Ultrathin sections of the medial part of the corpus callosum (cc) were analyzed by electron microscopy at P90 (WT n = 5; *Mct8/Dio2* KO n = 5) and P180 (WT n = 4; *Mct8/Dio2* KO n = 5). The number of myelinated axons was severely decreased in *Mct8/Dio2* KO mice as compared with WT animals. (b) Depicts the percentage of myelinated axons for each of the studied groups. No differences in the ultrastructure of the myelin sheaths were observed between both genotypes as seen in the higher-magnification insets (a) and in (c), which depicts the G ratio, calculated as (axon diameter)/(fiber diameter). Axon and fiber diameters were measured in 10 random axons per field (5 fields per animal). No significant differences were observed. Data are shown as box and whiskers plots (min to max). *$p < 0.05$, p values were determined by Kruskal-Wallis test. Scale bar represents 1 µm except in the insets, 250 nm.

MBP staining was lower in *Mct8/Dio2* KO mice compared to WT animals at P21 and P90 and the WM architecture was also affected with smaller tract size and abnormal definition of large axonal tracts, such as the cc. These observations are consistent with findings in other MCT8-deficient models, such as the *Mct8/Oatp1c1* double knock-out mice that presents decreased MBP staining from P12 to at least P120 and reduced width of the cc (Mayerl et al., 2014), and MCT8-deficient zebrafish models that present decreased *mbp* mRNA levels at the onset of myelination (Zada et al., 2014). An in-depth evaluation of the myelin status by TEM revealed that a high percentage of *Mct8/Dio2* KO mice brain axons

remain non-myelinated, even at late stages such as P180. However, the myelin sheaths of the effectively myelinated axons were no different from WT ones, which is also in agreement with findings in *Mct8/Oatp1c1* mice (Mayerl et al., 2014) and hypothyroid rats (Guadaño-Ferraz, 1992; Lucia et al., 2018). Moreover, myelination analysis by MRI in a model of MCT8 deficiency, provided for the first time in this study, indicate that this approach offers the possibility to perform long-term preclinical studies to evaluate the effect of potential therapeutic agents in improving the neurological impairments in MCT8 deficiency. This can be done by performing repeated measures throughout the treatment,
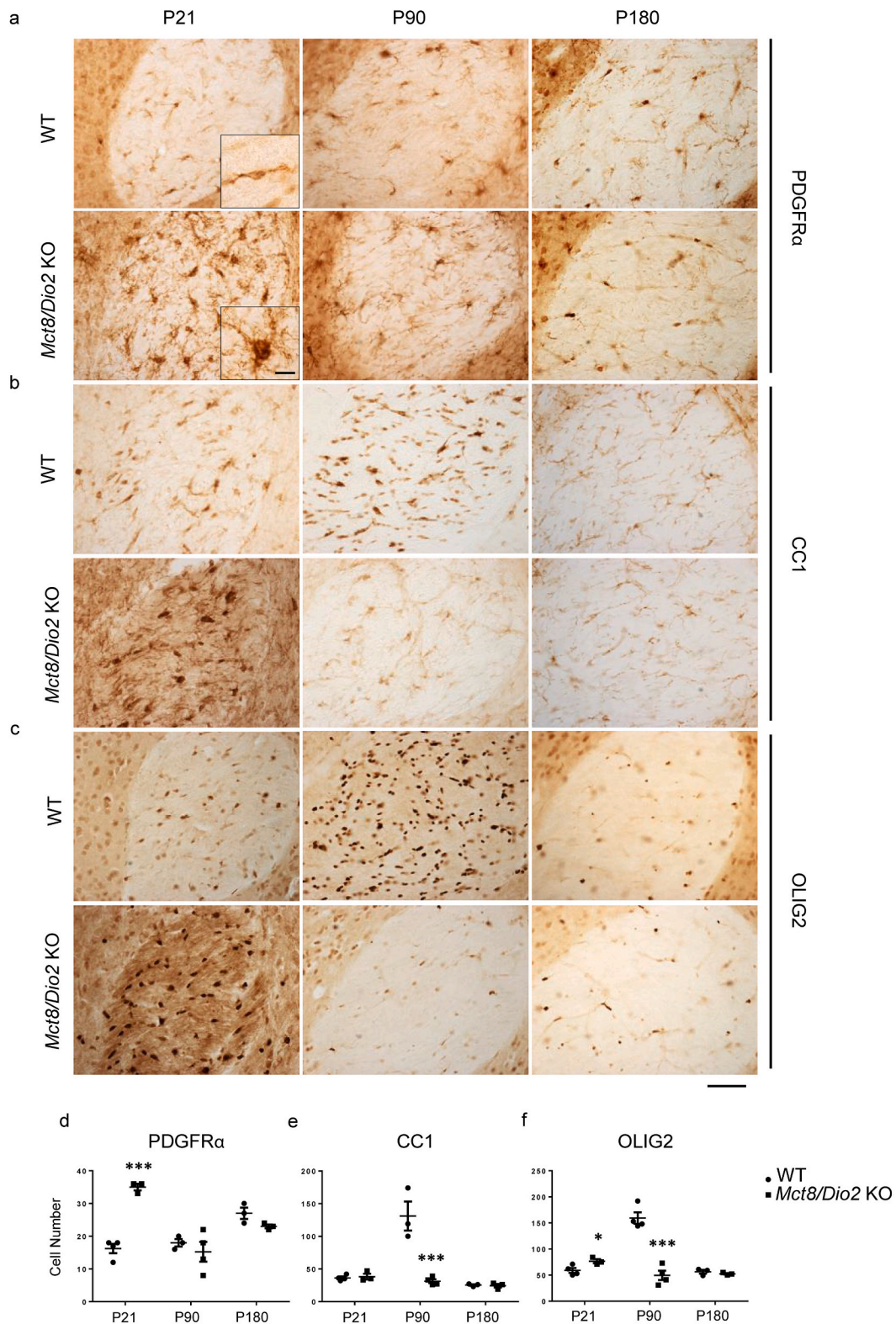
Fig. 8. Altered oligodendroglial development in *Mct8/Dio2* KO mice. Brain coronal sections of WT (n = 4) and *Mct8/Dio2* KO (n = 4) mice were immunostained PDGFRα (a), CC1 (b) and OLIG2 (c) at P21, P90 and P180. Representative images depict the immunostaining pattern in the anterior commissure. PDGFRα immunopositive cell density is higher at P21 in the *Mct8/Dio2* KO mice in comparison to WT animals, and this impairment improves throughout aging (a). CC1 immunopositive cell density is lower at P90 in *Mct8/Dio2* KO mice in comparison to WT mice and at P180 no differences can be observed between both genotypes (b). In comparison to WT mice, OLIG2 immunopositive cell density is higher at P21 in *Mct8/Dio2* KO mice, significantly lower at P90, and no differences can be observed at P180 (c). Insets in A depict PDGFRα positive cells in both WT and *Mct8/Dio2* KO mice. *Mct8/Dio2* KO mice OPCs show an aberrant increase of size and branching as compared to WT (see also Supplementary Fig. 4). Quantification of the number of positive PDGFRα OPCs (d), CC1 OLs (e) and OLIG2, as the entire oligodendroglial lineage (f) in the anterior commissure. Scale bar represents 125 μm except in the insets, 50 μm. OL: oligodendrocyte; OPC: oligodendrocyte precursor cell. Data are shown as box and whiskers plots (min to max). *$p > 0.05$ ***$p < 0.01$ was determined by two-way ANOVA.

using myelination as a biomarker, by non-invasive evaluations, instead of obtaining a single outcome in post-mortem samples.

Since the *Mct8/Dio2* KO mouse model reproduces the myelin impairments observed in AHDS patients, we have explored the OPCs and mature OLs population and we have found alterations in both populations. These analyses were performed in the ac, a white matter tract widely studied in relation to TH and myelin (Guadaño-Ferraz, 1992; Lucia et al., 2018), because it presents several advantages when performing cell counting quantification analysis in comparison to other brain regions that present several complications as it has been already addressed in literature (Riise and Pakkenberg, 2011). Similar studies in the entire cc and motor cortex will allow to directly compare the alterations in the oligodendroglial lineage cells and the myelin impairments observed in these regions. At early stages, *Mct8/Dio2* KO brains presented a higher density and aberrant morphology of OPCs population in comparison to WT, probably due to the lack of TH as a proliferation arrest cue, that reverted throughout aging. Moreover, *Mct8/Dio2* KO animals showed a highly reduced number of mature OLs at P90. This could be due to a combination of the reduced differentiation rate in the absence of TH (Baas et al., 1997; Billon et al., 2001) and increased OL apoptosis in the absence of MCT8 (Lee et al., 2017). Indeed, studies in Mct8-deficient zebrafish have also found reduced differentiation of OPCs into OLs (Zada et al., 2016) and it has been recently demonstrated that MCT8 is necessary both at the BBB and the OPCs membrane to facilitate their differentiation into mature OLs (Vatine et al., 2021). Future studies continuously tracing the fate of the OPCs and OLs populations in *Mct8/Dio2* KO mice will give further insights into the mechanisms that lead to alterations in the oligodendroglial linage.

Lastly, the myelin status in MCT8 deficiency has led to controversial interpretations mainly because different studies have reported either delayed or permanent hypomyelination. To address this it is essential to use a correct terminology, as already pointed out (Vancamp et al., 2020). "Permanent hypomyelination" is defined as an unchanged pattern of deficient myelination between two MRIs at least 6 months apart in a child older than 1 year (Pouwels et al., 2014; van der Knaap and Wolf, 2010) and "delayed myelination" refers to an improvement in myelination or WM content during this time interval (Schiffmann and van der Knaap, 2009). Regarding the MCT8-deficient patient studied in the present work, despite that MRI analysis did not detect myelination defects at 6.5 years of age, post-mortem histological analyses have revealed persistent myelination impairments at 11 years of age. All the above highlights the need to: 1) adopt an appropriate terminology to correctly and universally describe the myelin status in MCT8 deficiency. Even though it cannot be considered as hypomyelination by definition, it is very likely that there are permanent myelination impairments; 2) perform more sensitive and detailed analysis of the myelination status in MCT8 deficiency both by MRI and in post-mortem samples, whenever possible.

5. Conclusions

In the present work, we have further characterized the myelination impairments in MCT8 deficiency, both in a human patient and in *Mct8/Dio2* KO mice as a model of the syndrome. The present findings indicate that, even though the myelination impairments improve throughout age, there are still persistent myelination defects at later life stages although it cannot be strictly defined as hypomyelination. We have also identified a greater proportion of small-caliber axons in detriment of larger caliber ones, as well as impairments in oligodendroglial development as potential mechanisms underlying the myelination defects in MCT8 deficiency. These findings also indicate that therapeutic strategies aiming to improve the myelination impairments of MCT8-deficient patients should target both axonal-diameter-related processes and promote OPCs differentiation.

Data availability statement

The data that support the findings of this study are available from the corresponding authors upon reasonable request.

Declaration of Competing Interest

None.

Appendix A. Supplementary data

Supplementary data to this article can be found online at https://doi.org/10.1016/j.nbd.2021.105567.

References

Allan, W., Herndon, C.N., Dudley, F.C., 1944. Some examples of the inheritance of mental deficiency: apparently sex-linked idiocy and microcephaly. Am. J. Ment. Defic. 48, 325–334.

Almolda, B., Villacampa, N., Manders, P., Hidalgo, J., Campbell, I.L., González, B., Castellano, B., 2014. Effects of astrocyte-targeted production of interleukin-6 in the

mouse on the host response to nerve injury. Glia 62, 1142–1161. https://doi.org/10.1002/glia.22668.

Baas, D., Bourbeau, D., Sarliève, L.L., Ittel, M.E., Dussault, J.H., Puymirat, J., 1997. Oligodendrocyte maturation and progenitor cell proliferation are independently regulated by thyroid hormone. Glia 19, 324–332. https://doi.org/10.1002/(SICI)1098-1136(199704)19:4<324::AID-GLIA5>3.0.CO;2-X.

Bárez-López, S., Grijota-Martínez, C., Ausó, E., Fernández-De Frutos, M., Montero-Pedrazuela, A., Guadaño-Ferraz, A., 2019. Adult mice lacking Mct8 and Dio2 proteins present alterations in peripheral thyroid hormone levels and severe brain and motor skill impairments. Thyroid 29, 1669–1682. https://doi.org/10.1089/thy.2019.0068.

Bernal, J., 2005. Thyroid hormones and brain development. Vitam. Horm. 71, 95–122. https://doi.org/10.1016/S0083-6729(05)71004-9.

Bernal, J., Guadaño-Ferraz, A., Morte, B., 2015. Thyroid hormone transporters—functions and clinical implications. Nat. Rev. Endocrinol. 11, 406. https://doi.org/10.1038/nrendo.2015.66.

Billon, N., Tokumoto, Y., Forrest, D., Raff, M., 2001. Role of thyroid hormone receptors in timing oligodendrocyte differentiation. Dev. Biol. 235, 110–120. https://doi.org/10.1006/dbio.2001.0293.

Calzà, L., Fernández, M., Giardino, L., 2015. Role of the thyroid system in myelination and neural connectivity. Compr. Physiol. 5, 1405–1421. https://doi.org/10.1002/cphy.c140035.

Ceballos, A., Belinchon, M.M., Sanchez-Mendoza, E., Grijota-Martinez, C., Dumitrescu, A.M., Refetoff, S., Morte, B., Bernal, J., 2009. Importance of monocarboxylate transporter 8 for the blood-brain barrier-dependent availability of 3,5,3′-triiodo-L-thyronine. Endocrinology 150, 2491–2496. https://doi.org/10.1210/en.2008-1616.

Cheng, S.-Y., Leonard, J.L., Davis, P.J., 2010. Molecular aspects of thyroid hormone actions. Endocr. Rev. 31, 139–170. https://doi.org/10.1210/er.2009-0007.

Dumitrescu, A.M., Liao, X.-H., Best, T.B., Brockmann, K., Refetoff, S., 2004. A novel syndrome combining thyroid and neurological abnormalities is associated with mutations in a monocarboxylate transporter gene. Am. J. Hum. Genet. 74, 168–175. https://doi.org/10.1086/380999.

Friede, R.L., 1972. Control of myelin formation by axon caliber (with a model of the control mechanism). J. Comp. Neurol. 144, 233–252. https://doi.org/10.1002/cne.901440207.

Friesema, E.C.H., Ganguly, S., Abdalla, A., Manning Fox, J.E., Halestrap, A.P., Visser, T.J., 2003. Identification of monocarboxylate transporter 8 as a specific thyroid hormone transporter. J. Biol. Chem. 278, 40128–40135. https://doi.org/10.1074/jbc.M300909200.

Friesema, E.C.H., Grueters, A., Biebermann, H., Krude, H., von Moers, A., Reeser, M., Barrett, T.G., Mancilla, E.E., Svensson, J., Kester, M.H.A., Kuiper, G.G.J.M., Balkassmi, S., Uitterlinden, A.G., Koehrle, J., Rodien, P., Halestrap, A.P., Visser, T.J., 2004. Association between mutations in a thyroid hormone transporter and severe X-linked psychomotor retardation. Lancet (London, England) 364, 1435–1437. https://doi.org/10.1016/S0140-6736(04)17226-7.

Gika, A.D., Siddiqui, A., Hulse, A.J., Edward, S., Fallon, P., Mcentagart, M.E., Jan, W., Josifova, D., Lerman-sagie, T., 2018. White matter abnormalities and dystonic motor disorder associated with mutations in the SLC16A2 gene. Dev. Med. Child Neurol. 52, 475–482. https://doi.org/10.1111/j.1469-8749.2009.03471.x.

Gothié, J.D., Vancamp, P., Demeneix, B., Remaud, S., 2020. Thyroid hormone regulation of neural stem cell fate : from development to ageing. Acta Physiol. 1–24. https://doi.org/10.1111/apha.13316.

Grijota-Martínez, C., Bárez-López, S., Gómez-Andrés, D., Guadaño-Ferraz, A., 2020. MCT8 deficiency: the road to therapies for a rare disease. Front. Neurosci. 14, 1–8. https://doi.org/10.3389/fnins.2020.00380.

Guadaño-Ferraz, A., 1992. Desarrollo de la comisura anterior en la rata normal e hipotiroidea. Universidad Autónoma de Madrid.

Guadaño-Ferraz, A., del Rey, F.E., de Escobar, G.M., Innocenti, G.M., Berbel, P., 1994. The development of the anterior commissure in normal and hypothyroid rats. Dev. Brain Res. 81, 293–308. https://doi.org/10.1016/0165-3806(94)90315-8.

Kim, M.J., Petratos, S., 2019. Oligodendroglial lineage cells in thyroid hormone-deprived conditions. Stem Cells Int. 2019, 1–13. https://doi.org/10.1155/2019/5496891.

Kobayashi, S., Onuma, A., Inui, T., Wakusawa, K., Tanaka, S., Shimojima, K., Yamamoto, T., Haginoya, K., 2014. Clinical course and images of four familial cases of Allan-Herndon-Dudley syndrome with a novel monocarboxylate transporter 8 gene mutation. Pediatr. Neurol. 51, 414–416. https://doi.org/10.1016/j.pediatrneurol.2014.05.004.

La Piana, R., Vanasse, M., Brais, B., Bernard, G., 2015. Myelination delay and Allan-Herndon-Dudley syndrome caused by a novel mutation in the SLC16A2 gene. J. Child Neurol. 30, 1371–1374. https://doi.org/10.1177/0883073814555189.

Lee, J.Y., Kim, M.J., Deliyanti, D., Azari, M.F., Rossello, F., Costin, A., Ramm, G., Stanley, E.G., Elefanty, A.G., Wilkinson-Berka, J.L., Petratos, S., 2017. Overcoming monocarboxylate transporter 8 (MCT8)-deficiency to promote human oligodendrocyte differentiation and myelination. EBioMedicine 25, 122–135. https://doi.org/10.1016/j.ebiom.2017.10.016.

López-Espíndola, D., Morales-Bastos, C., Grijota-Martínez, C., Liao, X.-H., Lev, D., Sugo, E., Verge, C.F., Refetoff, S., Bernal, J., Guadaño-Ferraz, A., 2014. Mutations of the thyroid hormone transporter MCT8 cause prenatal brain damage and persistent hypomyelination. J. Clin. Endocrinol. Metab. 99, E2799–E2804. https://doi.org/10.1210/jc.2014-2162.

López-Espíndola, D., García-Aldea, Á., Gómez de la Riva, I., Rodríguez-García, A.M., Salvatore, D., Visser, T.J., Bernal, J., Guadaño-Ferraz, A., 2019. Thyroid hormone availability in the human fetal brain: novel entry pathways and role of radial glia. Brain Struct. Funct. 224, 2103–2119. https://doi.org/10.1007/s00429-019-01896-8.

Lucia, F.S., Pacheco-torres, J., González-granero, S., Canals, S., Obregón, M., García-verdugo, J.M., Berbel, P., Chan, K.C., 2018. Transient hypothyroidism during lactation arrests myelination in the anterior commissure of rats. A magnetic resonance image and electron microscope study. Front. Neuroanat. 12, 1–20. https://doi.org/10.3389/fnana.2018.00031.

Mayerl, S., Müller, J., Bauer, R., Richert, S., Kassmann, C.M., Darras, V.M., Buder, K., Boelen, A., Visser, T.J., Heuer, H., 2014. Transporters MCT8 and OATP1C1 maintain murine brain thyroid hormone homeostasis. J. Clin. Invest. 124, 1987–1999. https://doi.org/10.1172/JCI70324.

Papadimitriou, A., Dumitrescu, A.M., Papavasiliou, A., Fretzayas, A., Nicolaidou, P., Refetoff, S., 2007. A novel monocarboxylate transporter 8 gene mutation as a cause of severe neonatal hypotonia and developmental delay. Pediatrics 121, e199–e202. https://doi.org/10.1542/peds.2007-1247.

Pouwels, P.J.W., Vanderver, A., Bernard, G., Wolf, N.I., Dreha-kulczewksi, S.F., Deoni, S.C.L., Bertini, E., Richardson, W., 2014. Hypomyelinating leukodystrophies : translational research progress and prospects. Ann. Neurol. 5–19. https://doi.org/10.1002/ana.24194.

Remerand, G., Boespflug-Tanguy, O., Tonduti, D., Touraine, R., Rodriguez, D., Curie, A., Perreton, N., Des Portes, V., Sarret, C., Afenjar, A., Burglen, L., Castellotti, B., Cuntz, D., Desguerre, I., Doummar, D., Estienne, M., Freri, E., Heron, D., Moutard, M. L., Novara, F., Orcesi, S., Saletti, V., Zibordi, F., 2019. Expanding the phenotypic spectrum of Allan–Herndon–Dudley syndrome in patients with SLC16A2 mutations. Dev. Med. Child Neurol. 61, 1439–1447. https://doi.org/10.1111/dmcn.14332.

Riise, J., Pakkenberg, B., 2011. Stereological estimation of the total number of myelinated callosal fibers in human subjects. J. Anat. 218, 277–284. https://doi.org/10.1111/j.1469-7580.2010.01333.x.

Saab, A.S., Nave, K.A., 2017. Myelin dynamics: protecting and shaping neuronal functions. Curr. Opin. Neurobiol. 47, 104–112. https://doi.org/10.1016/j.conb.2017.09.013.

Schiffmann, R., van der Knaap, M.S., 2009. Invited article: an MRI-based approach to the diagnosis of white matter disorders. Neurology 72, 750–759. https://doi.org/10.1212/01.wnl.0000343049.00540.c8.

Sun, P., Murphy, R.K.J., Gamble, P., George, A., Song, S.K., Ray, W.Z., 2017. Diffusion assessment of cortical changes, induced by traumatic spinal cord injury. Brain Sci. 7, 1–13. https://doi.org/10.3390/brainsci7020021.

Valcana, T., Einstein, E.R., Csejtey, J., Dalal, K.B., Timiras, P.S., 1975. Influence of thyroid hormones on myelin proteins in the developing rat brain. J. Neurol. Sci. 25, 19–27. https://doi.org/10.1016/0022-510X(75)90183-5.

van der Knaap, M., Wolf, N., 2010. Hypomyelination versus delayed myelination. Ann. Neurol. 68, 2010. https://doi.org/10.1002/ana.21751.

Vancamp, P., Demeneix, B.A., Remaud, S., 2020. Monocarboxylate transporter 8 deficiency: delayed or permanent hypomyelination? Front. Endocrinol. (Lausanne) 11. https://doi.org/10.3389/fendo.2020.00283.

Vatine, G.D., Shelest, O., Mattis, V.B., Barriga, B.K., Heuer, H., Svendsen, C.N., 2021. Oligodendrocyte Progenitor Cell Maturation Is Dependent on Dual Function of MCT8 in the Transport of Thyroid Hormone across Brain Barriers and the Plasma Membrane, pp. 1–14. https://doi.org/10.1002/glia.24014.

Voyvodic, J.T., 1989. Target size regulates calibre and myelination of sympathetic axons. Nature 342, 430–433. https://doi.org/10.1038/342430a0.

Yano, R., Hata, J., Abe, Y., Seki, F., Yoshida, K., Komaki, Y., Okano, H., Tanaka, K.F., 2018. Quantitative temporal changes in DTI values coupled with histological properties in cuprizone-induced demyelination and remyelination. Neurochem. Int. 119, 151–158. https://doi.org/10.1016/j.neuint.2017.10.004.

Younes-Rapozo, V., Berendonk, J., Savignon, T., Manhães, A.C., Barradas, P.C., 2006. Thyroid hormone deficiency changes the distribution of oligodendrocyte/myelin markers during oligodendroglial differentiation in vitro. Int. J. Dev. Neurosci. 24, 445–453. https://doi.org/10.1016/j.ijdevneu.2006.08.004.

Zada, D., Tovin, A., Lerer-Goldshtein, T., Vatine, G.D., Appelbaum, L., 2014. Altered behavioral performance and live imaging of circuit-specific neural deficiencies in a zebrafish model for psychomotor retardation. PLoS Genet. 10 https://doi.org/10.1371/journal.pgen.1004615.

Zada, D., Tovin, A., Lerer-Goldshtein, T., Appelbaum, L., 2016. Pharmacological treatment and BBB-targeted genetic therapy for MCT8-dependent hypomyelination in zebrafish. DMM Dis. Model. Mech. 9, 1339–1348. https://doi.org/10.1242/dmm.027227.